Transition Metal Ion Mediated C-H and C-C Bond Activation of Alkanes: Dynamical Coupling between Entrance and Exit Channel Transition States

P. A. M. van Koppen,*,† J. Brodbelt-Lustig,† M. T. Bowers,† D. V. Dearden,‡ J. L. Beauchamp,‡ Ellen R. Fisher,§ and P. B. Armentrout*,§

Contribution from the Department of Chemistry, University of California, Santa Barbara, California 93106, Arthor Amos Noyes Laboratory of Chemical Physics,⊥ California Institute of Technology, Pasadena, California 91125, and the Department of Chemistry, University of Utah, Salt Lake City, Utah 84112. *Received August 20, 1990*

Abstract: The exothermic dihydrogen and methane loss channels for Co^+ reacting with propane, propane-*2*-d_1, propane-*2,2*-d_2, propane-*1,1,1*-d_3, propane-*1,1,1,3,3,3*-d_6, and propane-d_8 are examined. Measurements of the Co^+/C_3H_8 system with a guided ion beam apparatus yield a total cross section that is 13% of the Langevin collision cross section, with H_2 loss favored over CH_4 loss by a factor of 2.4. For Co^+ reacting with C_3D_8, the total cross section decreases by a factor of 2.8 relative to C_3H_8, but the branching ratio is unchanged. These results can be accommodated if both CH_4 loss and H_2 loss proceed via an initial C-H bond insertion that is rate limiting. Modeling with statistical phase space theory indicates that the barrier for C-H bond insertion is located 0.11 ± 0.03 eV below the Co^+/C_3H_8 asymptotic energy. Kinetic energy release distributions (KERDs) from nascent metastable $Co(C_3H_8)^+$ complexes were measured for H_2 loss and CH_4 loss. For H_2 loss the distribution is bimodal. Studies with propane-*2,2*-d_2 and propane-*1,1,1,3,3,3*-d_6 indicate that both primary and secondary C-H insertion are involved as initial steps. Initial secondary C-H insertion is responsible for the high-energy component in the bimodal KERD which is much broader than predicted from statistical theory, indicating that a tight transition state leads to the final products. The low-energy component for H_2 loss involves initial primary C-H insertion and appears to be statistical, suggesting little or no reverse activation barrier as the system separates to products. The kinetic energy distribution for demethanation, on the other hand, is narrower than predicted from unrestricted phase space theory calculations. Inclusion of the C-H insertion barrier into the calculation brings experiment and theory into excellent agreement. The barrier reduces the contribution of high angular momentum states to the final products, thus reducing the high-energy portion of the product kinetic energy distribution. This is the first documented example of a transition state remote from the exit channel strongly affecting product energy distributions.

I. Introduction

The growing use of mass spectrometric techniques[1] such as ion beams[2] and ion cyclotron resonance[3] for probing aspects of organotransition-metal reactions stems in part from the importance of organometallics as widely proposed intermediates in many catalytic transformations. In particular, considerable effort in recent years has been directed at understanding the mechanisms and energetics of C-H and C-C bond activation of alkanes by transition-metal ions.[4-11] Such exothermic ion-molecule reactions typically result in elimination of molecular hydrogen, alkanes, and alkenes, cleavages which are initiated by oxidative addition of a metal ion across a C-H or C-C bond. The initial insertion site has yet to be determined for many of these alkane elimination reactions.[5-11] Exothermic processes for Co^+ reacting with propane are exemplified in Scheme I.[2,5]

Propane is particularly interesting, since it is the smallest alkane to react with cobalt ions at thermal energies.[2] The lack of reactivity at thermal energies of the Co^+/C_2H_6 system is intriguing since recent measurements of the bond energy of $Co^+-(C_2H_4)$ indicate that this H_2 elimination is exoergic.[12,13] Georgiadis et al.[2d] observe this reaction, but with a threshold. The threshold energy is not precisely characterized because of the small size of the cross section, but it is less than 1 eV. At higher kinetic energies $(CoCH_3)^+ + CH_3$ and $(CoH)^+ + C_2H_5$ are the dominant reaction channels. Under multicollision conditions, Weisshaar et al.[6] find that Co^+ reacts with CH_4 and C_2H_6 *only* by adduct formation and with C_3H_8 primarily by adduct formation.

For Co^+ reacting with propane under single-collision conditions at thermal energies, two exoergic product channels are observed[2d] (as exemplified in Scheme I). H_2 elimination is favored over CH_4 loss by about a factor of 3. The total reaction cross section is only about 13%[2d] of the Langevin-Gioumousis-Stevenson[14] (LGS) limit. Hence, even though the reactions proceed at low energy, efficient reaction is precluded for either entropic or energetic reasons.

Scheme I

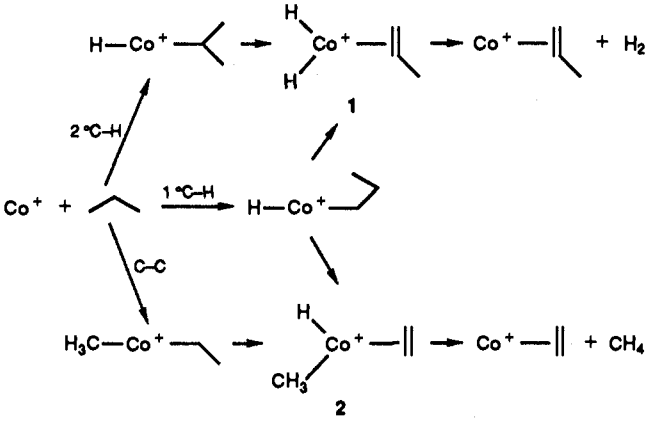

† University of California.
‡ California Institute of Technology.
§ University of Utah.
⊥ Contribution No. 8122.

(1) For a recent review see: Allison, J. In *Progress in Inorganic Chemistry*; Lippard, S. J., Ed.; Wiley-Interscience: New York, 1986; p 627 and references therein.
(2) See for example: (a) Armentrout, P. B.; Beauchamp, J. L. *J. Am. Chem. Soc.* **1981**, *103*, 784. (b) Elkind, J. L.; Armentrout, P. B. *J. Phys. Chem.* **1985**, *89*, 5626. (c) Sunderlin, L.; Aristov, N.; Armentrout, P. B. *J. Am. Chem. Soc.* **1987**, *109*, 78. (d) Georgiadis, R.; Fisher, E. R.; Armentrout, P. B. *J. Am. Chem. Soc.* **1989**, *111*, 4251.
(3) See for example: (a) Allison, J.; Freas, R. B.; Ridge, D. P. *J. Am. Chem. Soc.* **1979**, *101*, 1332. (b) Larson, B. S.; Ridge, D. P. *J. Am. Chem. Soc.* **1984**, *106*, 1912. (c) Uppal, J. S.; Staley, R. H. *J. Am. Chem. Soc.* **1982**, *104*, 1238. (d) Byrd, G. D.; Burnier, R. C.; Freiser, B. S. *J. Am. Chem. Soc.* **1982**, *104*, 3565. (e) Jacobson, D. B.; Freiser, B. S. *Organometallics* **1984**, *3*, 513. (f) Huang, Y.; Freiser, B. S. *J. Am. Chem. Soc.* **1989**, *111*, 2387.
(4) Tolbert, M. A.; Beauchamp, J. L. *J. Am. Chem. Soc.* **1984**, *106*, 8117.
(5) Schultz, R. H.; Elkind, J. L.; Armentrout, P. B. *J. Am. Chem. Soc.* **1988**, *110*, 411.
(6) Tonkyn, R.; Ronan, M.; Weisshaar, J. C. *J. Phys. Chem.* **1988**, *92*, 92.
(7) Jacobson, D. B.; Freiser, B. S. *J. Am. Chem. Soc.* **1983**, *105*, 5197.
(8) Houriet, R.; Halle, L. F.; Beauchamp, J. L. *Organometallics* **1983**, *2*, 1818.

0002-7863/91/1513-2359$02.50/0

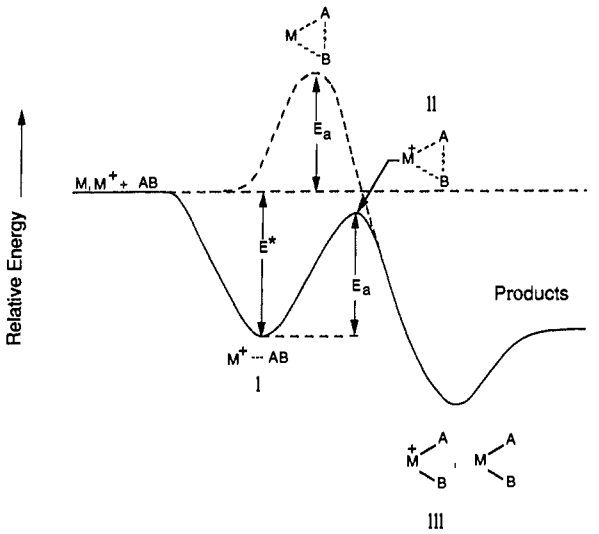

Figure 1. Schematic reaction coordinate diagram comparing the difference between metal atoms and metal ions inserting into a bond as a first step in a chemical reaction. The electrostatic attractive well of the $M(AB)^+$ complex can completely offset the insertion barrier if $E^* > E_a$.

Butanes and larger alkanes, on the other hand, react on essentially every collision with Co^+.[2a] As the systems increase in size additional reaction channels become available, but H_2 and CH_4 loss are still efficient processes. An interesting question is posed as to why propane and higher alkanes are reactive and ethane is not. The C–H and C–C bond energies are very similar in each of these systems,[2d,15] and consequently, any barriers to insertion by the metal ion should be similar. A possible answer to this question is given by the schematic potential energy surface in Figure 1. In neutral systems a significant barrier to reaction is usually associated with the activation of C–H or C–C bonds at coordinatively unsaturated transition-metal centers.[16] Ions, on the other hand, interact with neutrals via charge-induced dipole forces creating a chemically activated adduct with sufficient internal energy to overcome intrinsic barriers for insertion into C–H or C–C bonds, as shown in Figure 1. In reactions of Co^+ with alkanes, a reasonable explanation for the increased reactivity with alkane size is the increasing polarizability of the neutral. As the polarizability of the neutral becomes larger the depth of the initial electrostatic potential well deepens, eventually overcoming the intrinsic barrier to bond insertion.

A second, and perhaps more fundamental, question is whether C–H, C–C, or both C–H and C–C bonds are involved in the initial activation step by the metal ion. The goals of this paper are to determine if there is a barrier along the reaction coordinate in the Co^+/propane system; if so, what is its magnitude; and is the barrier associated with C–H insertion, C–C insertion, or both? Further, what is the relative importance of primary and secondary initial C–H insertion?

Our approaches to these problems are several. The principal method involves accurate measurement of kinetic energy release distributions for the two product channels. Measurements of this type have provided both energetic and mechanistic details for similar systems.[12,13] Selectively deuterated propanes are used to assist in the mechanistic interpretations. These studies are augmented by guided ion beam experiments in which absolute cross sections are measured for the various reaction channels. Such measurements indicate how efficient a reaction is and how that efficiency changes with both deuterium substitution and collision energy. Finally, statistical phase space theory[17,18] will be applied to both sets of experiments. Phase space theory has been successfully used to model kinetic energy release distributions for reactions with no reverse activation barriers.[12,13,18] It has also been very successful in modeling barriers along the reaction coordinate and determining their height relative to the entrance channel energy.[19] Both applications will be used here in an effort to uncover the detailed mechanisms of these reactions.

Table I. Co^+ + Propanes

system	total cross section,[a] (Å^2)	$(\sigma_{tot}/\sigma_{LGS})^b$	adduct lifetime,[d] μs
C_3H_8	23[c]	0.13 ± 0.05	0.45
CH_3CHDCH_3	20 ± 2	0.11 ± 0.01	0.50
$CH_3CD_2CH_3$	21 ± 4	0.12 ± 0.02	0.52
$CD_3CH_2CH_3$	24 ± 2	0.14 ± 0.01	0.65
$CD_3CH_2CD_3$	16 ± 4	0.09 ± 0.02	1.50
C_3D_8	8 ± 2	0.05 ± 0.02	1.60

[a] Total cross section for methane and dihydrogen elimination measured at 0.05 eV. Loss of propane is not included. The uncertainties indicated for the labeled propane systems are relative to the C_3H_8 system. [b] σ_{LGS} is the Langevin collision cross section. [c] The absolute uncertainty in the total cross section for the C_3H_8 system is ±10 Å^2.[23] [d] These represent lower limits of the lifetime.[4]

II. Experimental Section

Metastable kinetic energy release distributions were measured at UCSB using a reverse geometry double focusing mass spectrometer (VG Instruments ZAB-2F)[20] with a home-built variable-temperature EI/CI source. Metal ions were formed by electron impact (150 eV) on $Co(CO)_3NO$. Typical source pressures were 10^{-3} Torr, and source temperatures were kept below 280 K to minimize decomposition of $Co(CO)_3NO$ on insulating surfaces.

The organometallic ions were formed in the ion source by reaction of the bare metal ions with the organic neutrals. The ion source was operated at near field free conditions to prevent kinetic excitation of ions. The ions were accelerated to 8 kV after leaving the source and mass analyzed using a magnetic sector. Metastable ions decomposing in the second field free region between the magnetic and electric sectors were energy analyzed by scanning the electric sector. The sampled ions are those which decompose approximately 10 ± 5 μs after exiting the ion source. The metastable peaks were collected with a multichannel analyzer and differentiated to yield kinetic energy release distributions.[21] Integrated peak areas were used to obtain the product distributions. The resolution of the main beam was sufficient to avoid contribution to the metastable peak widths.

The ion beam results were obtained on the Utah guided ion beam apparatus, which has been described in detail previously.[22] Co^+ is formed by surface ionization, such that the ions are largely in their ^3F ground state (85%) but with a 15% contribution from the ^5F first excited state.[2d] The ions are focused into a magnetic sector for mass analysis, decelerated to a desired kinetic energy, and injected into an octopole ion guide. The octopole passes through a static gas cell into which the reactant gas is introduced. Pressures are maintained at a sufficiently low level (<0.1 mTorr) that multiple ion–molecule collisions are improbable. Product and unreacted beam ions are contained in the guide until they

(9) Armentrout, P. B.; Beauchamp, J. L. *Acc. Chem. Res.* **1989**, *22*, 315.
(10) Armentrout, P. B. In *Gas Phase Inorganic Chemistry*; Russel, D., Ed.; Plenum: New York, 1989; p 1.
(11) See: (a) Schulze, C.; Schwarz, H.; Peake, D. A.; Gross, M. L. *J. Am. Chem. Soc.* **1987**, *109*, 2368 and references therein. (b) Schwarz, H. *Acct. Chem. Res.* **1989**, *22*, 282.
(12) (a) Hanratty, M. A.; Beauchamp, J. L.; Illies, A. J.; Bowers, M. T. *J. Am. Chem. Soc.* **1985**, *107*, 1788. (b) Hanratty, M. A.; Beauchamp, J. L.; Illies, A. J.; van Koppen, P. A. M.; Bowers, M. T. *J. Am. Chem. Soc.* **1988**, *110*, 1.
(13) (a) van Koppen, P. A. M.; Jacobson, D. B.; Illies, A. J.; Bowers, M. T.; Hanratty, M. A.; Beauchamp, J. L. *J. Am. Chem. Soc.* **1989**, *111*, 1991. (b) van Koppen, P. A. M.; Bowers, M. T.; Beauchamp, J. L. *Organometallics* **1990**, *9*, 625.
(14) Gioumousis, G.; Stevenson, D. P. *J. Chem. Phys.* **1958**, *29*, 294.
(15) Cox, J. D.; Pilcher, G. *Thermochemistry of Organic and Organometallic Compounds*; Academic Press: New York, 1970.
(16) Crabtree, R. H. *Chem. Rev.* **1985**, *85*, 245.
(17) (a) Pechukas, P.; Light, J. C.; Rankin, C. *J. Chem. Phys.* **1966**, *44*, 794. (b) Nikitin, E. *Theor. Exp. Chem. (Engl. Tansl.)* **1965**, *1*, 285.
(18) (a) Chesnavich, W. J.; Bowers, M. T. *J. Am. Chem. Soc.* **1976**, *98*, 8301. (b) Chesnavich, W. J.; Bowers, M. T. *J. Chem. Phys.* **1978**, *68*, 901. (c) Chesnavich, W. J.; Bowers, M. T. *Prog. Reaction Kinet.* **1982**, *11*, 137.
(19) (a) Bass, L. M.; Cates, R. D.; Jarrold, M. F.; Kirchner, N.; Bowers, M. T. *J. Am. Chem. Soc.* **1983**, *105*, 7024. (b) Jarrold, M. F.; Bowers, M. T.; DeFrees, D. J.; McLean, A. D.; Herbst, E. *Astrophys. J.* **1986**, *303*, 392. Wagner-Redeker, W.; Kemper, P. R.; Jarrold, M. F.; Bowers, M. T. *J. Chem. Phys.* **1985**, *83*, 1121.
(20) Morgan, R. P.; Beynon, J. H.; Bateman, R. H.; Green, B. N. *Int. J. Mass Spectrom. Ion Phys.* **1978**, *28*, 171.
(21) (a) Jarrold, M. F.; Illies, A. J.; Bowers, M. T. *Chem. Phys.* **1982**, *65*, 19. (b) Kirchner, N. J.; Bowers, M. T. *J. Phys. Chem.* **1987**, *91*, 2573.
(22) Ervin, K. M.; Armentrout, P. B. *J. Chem. Phys.* **1985**, *83*, 166.

Table II. Branching Ratios for Reaction of Co^+ with Isotopically Substituted Propanes[a]

neutral products	C_3H_8	CH_3CHDCH_3	$CH_3CD_2CH_3$	$CH_3CH_2CD_3$	$CD_3CH_2CD_3$	C_3D_8
H_2	77 (2)	48 (2)	4 (2)[c]	53 (2)	4 (2)[c]	
HD		27 (2)	64 (2)	27 (2)	73 (5)	
D_2			4 (2)[c]	2 (2)[c]	9 (5)	77 (2)
total	77 (2)[b]	75 (2)	72 (3)	82 (2)	86 (2)	77 (2)
CH_4	23 (2)	23 (1)	26 (1)			
CH_3D		2 (1)[c]	2 (1)[c]	7 (1)		
CD_2H_2				<1 (1)[c]		
CD_3H				11 (1)	1 (1)[c]	
CD_4					13 (1)	23 (2)
total	23 (2)	25 (2)	28 (2)	18 (2)	14 (2)	23 (2)

[a] Measurements taken at 0.05 eV. The numbers in parentheses indicate the uncertainties. [b] The branching ratio for the C_3H_8 system represents the average values for three data sets which were taken at the same time as the various deuterated propanes. The average value including earlier data sets is 71 ± 4.[23] [c] These products could not be corrected unambiguously for the possibility of mass overlap from adjacent intense products and therefore could be substantially smaller or zero.

leave the gas cell. The ions are then focused into a quadrupole mass filter for product mass analysis and detected by means of a scintillation ion counter. Raw ion intensities are converted to absolute cross sections as described previously.[22]

The absolute energy and the energy distribution of the ions are measured by using the octopole as a retarding field analyzer. The fwhm of the energy distribution is generally 0.5 eV in the laboratory frame for these reactions. Uncertainties in the absolute energy scale are ±0.05 eV lab. Translational energies in the laboratory frame of reference are related to energies in the center of mass (CM) frame by $E_{CM} = E_{lab}m/(M + m)$, where M and m are the masses of the incident ion and neutral reactant, respectively.

All compounds were obtained commercially and admitted to the mass spectrometer after several freeze–pump–thaw cycles to remove noncondensable gases. The deuterated hydrocarbons were obtained from Merck, Sharpe and Dohme. The stated minimum isotopic purities were 98% for all the labeled propanes except for $CD_3CD_2CD_3$ which was 99% pure.

III. Results

Absolute cross-section measurements were obtained using a guided ion beam apparatus[5,22] for reactions of Co^+ with propane, propane-*2*-d_1, propane-*2,2*-d_2, propane-*1,1,1*-d_3, propane-*1,1,1,3,3,3*-d_6, and propane-d_8. Absolute cross-section measurements at low energies (<0.1 eV) and relative uncertainties are listed in Table I for all of the propane systems studied here. The uncertainty in the absolute cross section[23] based on reproducibility for the C_3H_8 system is ±10 Å^2. The total reaction cross sections relative to the Langevin collision cross sections at 0.05 eV are also summarized in Table I. Total cross sections for Co^+ induced dehydrogenation and demethanation of C_3H_8 and C_3D_8 as a function of kinetic energy are shown in Figure 2. These results represent the averages of several determinations (3–8 data sets). The results of Figure 2 and Table I illustrate that the absolute cross sections at low kinetic energy decrease as the extent of deuteration increases.

Formation of a $Co(C_3H_8)^+$ adduct was also observed in these studies and was found to increase with the extent of deuteration. Pressure-dependent studies of these cross sections demonstrated that these adducts were collisionally stabilized species, and also that the dehydrogenation and demethanation cross sections were pressure independent. These data were analyzed using the method outlined by Tolbert and Beauchamp[4] to derive lifetimes for the adduct species at a kinetic energy of 0.07 eV. These are listed in Table I and can be seen to increase as the extent of deuteration increases. These results are in line with the fact that the density of states increases as the extent of deuteration increases. For the C_3H_8 system, adduct formation is negligible at the pressures typically used to obtain cross-section data (0.05 mTorr).

The guided ion beam studies also delineate the branching ratios at the lowest energies (0.05–0.1 eV) between the two exothermic channels in the reaction of Co^+ with all of the propanes (Table II). For all of the systems, H_2 elimination is favored over CH_4 elimination at the lowest energies. As the kinetic energy is increased, the fraction of dehydrogenation product decreases until ~0.5 eV C.M. where demethanation becomes the dominant channel as shown in Figure 3. At low energies the branching ratio between the channels depends on where the propane is deuterated. For C_3H_8 and C_3D_8, dehydrogenation is favored over demethanation by about a factor of 3.3 (Table II). For deuteration

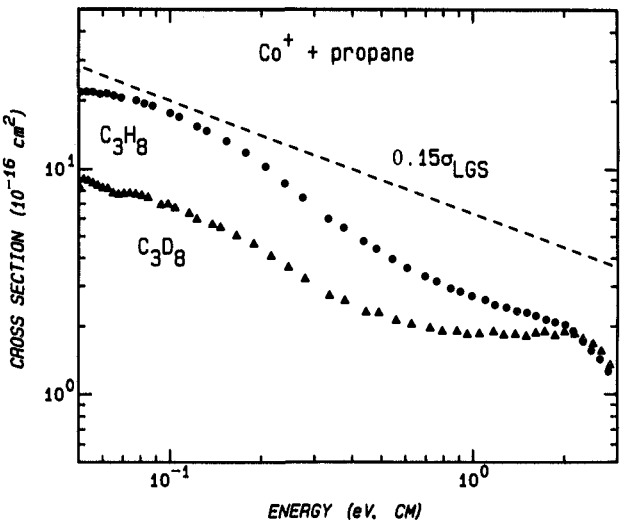

Figure 2. Variation of total cross section for dehydrogenation and demethanation as a function of kinetic energy in the center-of-mass frame for the reaction of Co^+ with propane and propane-d_8. The dashed line shows 15% of the collision cross section, σ_{LGS}, given by $\sigma_{LGS} = \pi e(2\alpha/E)^{1/2}$, where α is the polarizability of propane (6.23 Å^3).

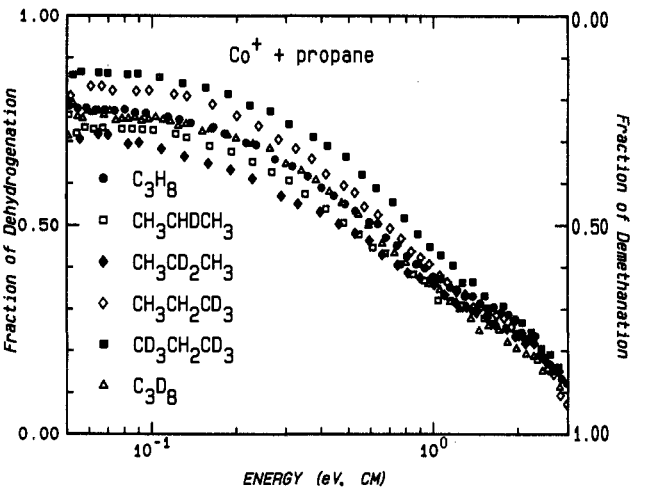

Figure 3. Variation in the fraction of the total cross section due to the hydrogen-loss channel as a function of kinetic energy in the center-of-mass frame for the reaction of Co^+ with propane (closed circles), propane-*2*-d_1 (open squares), propane-*2,2*-d_2 (closed diamonds), propane-*1,1,1*-d_3 (open diamonds), propane-*1,1,1,3,3,3*-d_6 (closed squares), and propane-d_8 (open triangles). The right-hand vertical scale corresponds to the fraction of the total cross section due to the methane-loss channel.

Table III. Product Distributions of Metastable Reactions of Nascent $Co(C_3H_8)^+$ Complexes

neutral product	metastable ion				
	$Co(C_3H_8)^+$	$Co(CH_3CHDCH_3)^+$	$Co(CH_3CD_2CH_3)^+$	$Co(CD_3CH_2CD_3)^+$	$Co(C_3D_8)^+$
H_2	65	46	<1		
HD		18	40	43	
D_2					28
CH_4	3	3	4		
CH_3D			0		
CD_4				1	<1
$C_3H_nD_{8-n}$[a]	32	33	55	56	72

[a] Elimination of propane.

Table IV. Reaction Enthalpies and Average Kinetic Energy Releases from Experiment and Phase Space Theory

			$-\Delta H$,[a] eV	$\bar{E}_t$, eV	
				expt	theory[b]
$Co^+ + C_3H_8$	→	$Co(C_3H_6)^+ + H_2$	0.71	0.33	0.10
$Co^+ + CH_3CD_2CH_3$	→	$Co(C_3H_5D)^+ + HD$	0.71	0.24	0.11
$Co^+ + CH_3CD_2CH_3$	→	$Co(C_3H_4D_2)^+ + H_2$	0.71[c]	0.75	0.11
$Co^+ + C_3D_8$	→	$Co(C_3D_6)^+ + D_2$	0.71	0.24	0.11
$Co^+ + C_3H_8$	→	$Co(C_2H_4)^+ + CH_4$	1.04	0.099	0.10[d] (0.15)[e]
$Co^+ + C_3D_8$	→	$Co(C_2D_4)^+ + CD_4$	1.04	0.098	0.094[f]

[a] Heat of reaction at 0 K, deuterium effects are assumed negligible. [b] Statistical phase space theory using the methods outlined in ref 11b. [c] Heat of reaction assuming the Co(propene)$^+$ product ion structure. For the cobaltacyclobutane product ion the reaction is endothermic by 0.47 eV. [d] Statistical phase space theory with a barrier for initial C–H bond insertion located 0.11 eV below the Co^+/C_3H_8 asymptotic energy, as described in the model in this paper. [e] Statistical phase space theory without a C–H insertion barrier included. [f] Statistical phase space theory with a barrier for initial C–H bond insertion located 0.06 eV below the Co^+/C_3D_8 asymptotic energy.

at the end carbons, $CH_3CH_2CD_3$ and $CD_3CH_2CD_3$, this ratio increases to 4.5 and 6.1, respectively. These results suggest that deuteration at a primary carbon enhances loss of hydrogen relative to demethanation. Deuteration at the central carbon has a much smaller but opposite effect, with this ratio decreasing to 3.0 and 2.8 for CH_3CHDCH_3 and $CH_3CD_2CH_3$, respectively. These results again represent the averages of several data sets taken at different times.

Table II also shows the branching ratios for the isotopically labeled products eliminated for the individual channels (dehydrogenation and demethanation). For CH_3CHDCH_3 and $CH_3CH_2CD_3$, H_2 loss is favored over HD loss by a factor of ~2, whereas for $CH_3CD_2CH_3$ and $CD_3CH_2CD_3$, HD loss is nearly 90% of the dehydrogenation product. For CH_3CHDCH_3 and $CH_3CD_2CH_3$, CH_4 accounts for nearly all of the methane-loss channel, with small amounts of CH_3D loss. For $CD_3CH_2CD_3$, more than 90% of the methane-loss channel is CD_4 loss, with <10% contribution from CD_3H. In the case of $CH_3CH_2CD_3$, there is about a 2:1 ratio between CD_3H loss and CH_3D loss.

Metastable decomposition reactions of nascent Co^+ complexes with propane, propane-*2*-d_1, propane-*2,2*-d_2, propane-*1,1,1,3,3,3*-d_6, and propane-d_8 were studied. The observed metastable product distributions are summarized in Table III.

Statistical phase space theory is used to model both the absolute cross sections and the experimental kinetic energy release distributions. The calculations have been previously described.[12,13,18,19] One purpose of the calculations is to determine whether a statistical model, which assumes a potential energy surface without a barrier to the reverse association in the exit channel, is adequate to describe the experimental kinetic energy release distribution. The calculated and experimental average kinetic energy releases, $\bar{E}_t$, are presented in Table IV. A second purpose of the calculations is to model the potential energy surface and determine, if possible, the nature and energies of important tight transition states the system encounters.[19] The parameters used in the phase space calculations are summarized in Appendix A.

The kinetic energy release distribution for H_2 loss from Co-$(C_3H_8)^+$ is bimodal as shown in Figure 4. This contrasts with the very narrow KERD calculated by using phase space theory also shown in Figure 4.[24]

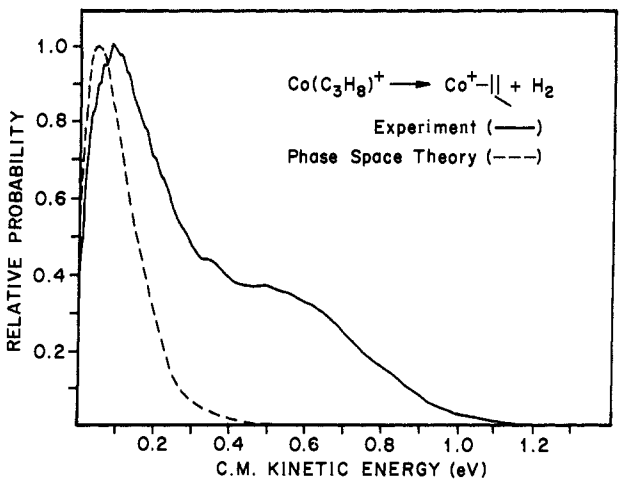

Figure 4. Kinetic energy release distribution for metastable loss of H_2 from nascent $Co(C_3H_8)^+$ collision complexes. The solid line labeled "experiment" results from analysis of the laboratory peak shape using the standard techniques (ref 21). The dashed line results from phase space theory calculations, including a barrier for initial C–H insertion (see text).

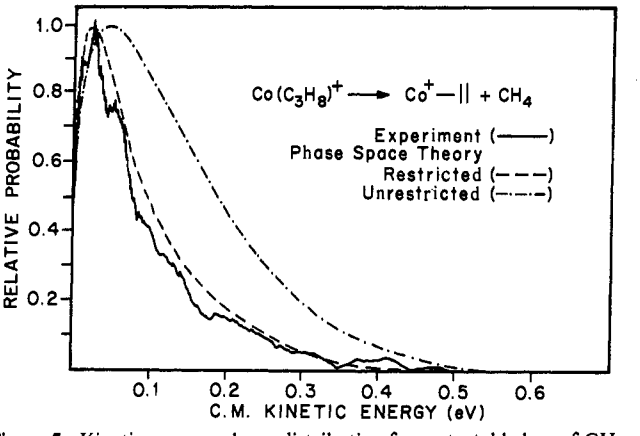

Figure 5. Kinetic energy release distribution for metastable loss of CH_4 from nascent $Co(C_3H_8)^+$ collision complexes. The "unrestricted" phase space theory curve assumes the entrance channel contains only an orbiting transition state, the exit channel has only an orbiting transition state (no reverse activation barrier), and there are no tight transition states in between that affect the dynamics. The "restricted" phase space theory calculation includes a tight transition state for insertion into a C–H bond located 0.11 eV below the asymptotic energy of the reactants (see text).

The kinetic energy release distribution for CH_4 loss from Co-$(C_3H_8)^+$ is shown in Figure 5. The observed distribution is

(23) The large uncertainty in the reaction cross-section measurements is due to the extreme sensitivity of this system to experimental conditions. Slight changes in the thermal energy distribution of the reactant may dramatically change the absolute cross section. However, relative branching ratios for all the labeled species were reproduced with much greater accuracy since these were measured under the same experimental conditions.

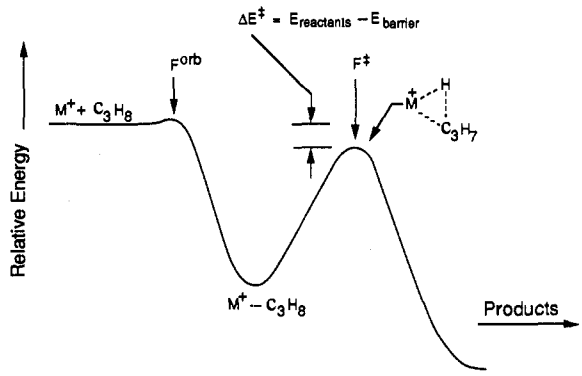

Figure 6. A schematic reaction coordinate diagram for insertion of Co^+ into a C–H bond of C_3H_8. The fluxes through the orbiting and tight transition states are depicted as F^{orb} and $F^{\ddagger}$, respectively.

narrower than that predicted by unrestricted statistical phase space theory. This is a very unusual result and suggests some interesting dynamics are occurring in this reaction. Aspects of the potential energy surfaces that could lead to these dynamics are discussed below. The kinetic energy release distribution for CH_4 loss from $Co(C_3H_8)^+$ was measured as a function of the accelerating voltage (8 and 4 kV). The shape of the distribution was independent of the accelerating voltage used. This is indicative of a narrow range of internal energies undergoing metastable decomposition relative to the total available energy.

IV. Discussion

A. Absolute Cross-Section Measurements for Co^+/Propane. The absolute cross-section data for reaction of Co^+ with C_3H_8 indicate that H_2 loss is favored over CH_4 loss by approximately a factor of 3 at the lowest energy studies (~0.05 eV C.M.). Interestingly, as the kinetic energy increases, the CH_4-loss channel becomes relatively enhanced until it becomes favored at ~0.5 eV C.M. and becomes dominant at energies above 2.0 eV C.M., as shown in Figure 3. One possible explanation for this behavior is that CH_4 loss can come from two mechanisms: initial C–H bond insertion followed by β-CH_3 transfer and by initial C–C bond insertion followed by β-H transfer as shown in Scheme I. Initial C–C bond insertion is not likely to be prevalent at the lowest energies, however, since perdeuterating C_3H_8 decreases the cross sections for *both* H_2 loss and CH_4 loss by precisely the same amount. These results strongly suggest that at low energies C–H bond insertion is the exclusive initial step in the reaction sequence and that the H_2-loss or CH_4-loss partitioning occurs further along the reaction coordinate. It seems likely that a barrier exists to initial C–C bond insertion and that this reaction channel opens up at higher collision energies as suggested previously.[2d]

The fact that the total cross section for Co^+ reacting with propane is 13% of the Langevin limit at thermal energies suggests that both H_2 loss and CH_4 loss are inefficient despite being exoergic. It is also intriguing that deuteration substantially decreases the total cross section (by a factor of about 3 for C_3D_8 (Figure 2) and by a lesser amount for the other deuterated propanes (see Table I)). A quantitative theoretical model that explains these observations is given next.

1. Model Potential Energy Surface for C–H Insertion. Exoergic ion–molecule reactions that are relatively inefficient are fairly well-known. The qualitative model developed to explain this observation is similar to the picture shown in Figure 1; the collision results in an initial electrostatic potential well followed by a tight transition state that restricts the flow of reactants to products.[19,25] Quantitative statistical phase space theory modeling using this simple idea has been done for a number of systems.[19] Details are given in the Appendix.

(24) The high-energy tail in Figure 4 is reduced somewhat if a more sophisticated method is used to account for instrument discrimination in obtaining the kinetic energy release distribution. See for example: Rumpf, B. A.; Derrick, P. J. *Int. J. Mass Spectrom. Ion Proc.* **1988**, *82*, 239. This however does not affect the interpretation of the results presented in this paper.

(25) Olmstead, W. N.; Brauman, J. I. *J. Am. Chem. Soc.* **1977**, *99*, 4219.

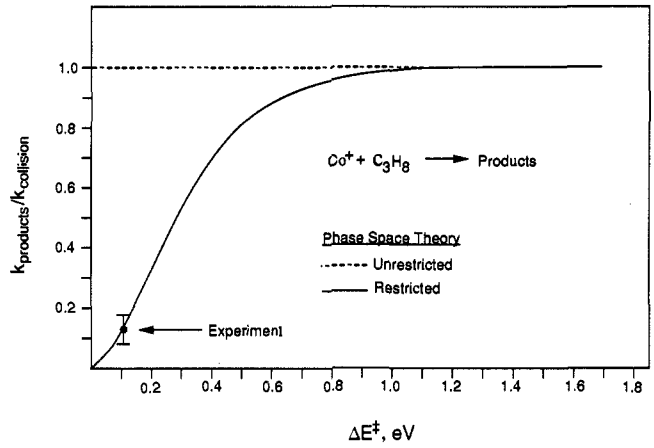

Figure 7. A plot of the total reaction efficiency, $k_{products}/k_{collision}$, for reaction of Co^+ with C_3H_8 versus $\Delta E^{\ddagger}$ (defined in Figure 6). The "unrestricted" phase space theory result (dashed line) assumes the tight transition state for C–H bond insertion does not affect the kinetics of the reaction. The "restricted" phase space theory calculation (solid line) incorporates the C–H insertion barrier into the analysis.

A reaction coordinate diagram defining the important parameters is given in Figure 6. Metal ions collide with propane neutrals and form the activated $Co(C_3H_8)^+$ electrostatic complex. This complex, once formed, can either pass through the tight transition state and proceed to products or pass back through the orbiting transition state and return to reactants. The energetic placement of the C–H insertion barrier relative to the Co^+/C_3H_8 reactant asymptotic energy will depend on the depth of the electrostatic well. For ions and nonpolar neutral molecules the attractive part of this insertion is dominated by the polarization energy

$$V(r) = -\frac{\alpha q^2}{2r^4} \tag{1}$$

where α is the polarizability of the neutral, q the charge on the ion, and r the ion–neutral separation. As the size of the neutral increases, α increases and the magnitude of $V(r)$ increases. At some molecular size, $V(r)$ will exceed the intrinsic height of the C–H insertion barrier and insertion will become exoergic. For Co^+/alkane systems this appears to occur for C_3H_8.

The reaction can be schematically written

$$Co^+ + C_3H_8 \underset{k_{orb}(E,J)}{\overset{k_{collision}p(E,J)}{\rightleftharpoons}} [Co(C_3H_8)^+]^* \xrightarrow{k^{\ddagger}(E,J)} \text{products} \tag{2}$$

The rate constant for product formation can be written

$$k_{products} = k_{collision} \int_E \int_J p(E,J) \frac{k^{\ddagger}(E,J)}{k^{\ddagger}(E,J) + k_{orb}(E,J)} \, dE \, dJ \tag{3}$$

where $k_{collision}$ is the Langevin collision rate constant for formation of $[Co(C_3H_8)^+]^*$, $p(E,J)$ is the distribution of energy and angular momentum states of $[Co(C_3H_8)^+]^*$ created by passage of the reactants through the orbiting transition state in the entrance channel, and $k_{orb}(E,J)$ and $k^{\ddagger}(E,J)$ are respectively the microscopic rate constants for passage through the orbiting transition state leading back to reactants and the tight transition state that eventually leads to products. Details of the microcanonical approach used are given in the Appendix. Of importance here is the fact that both $k_{orb}(E,J)$ and $k^{\ddagger}(E,J)$ are strong functions of E and J. Further, $k^{\ddagger}(E,J)$ will depend strongly on the height of the insertion barrier shown in Figure 6, and hence on $\Delta E^{\ddagger}$, the energy difference between the asymptotic energy of the reactants and the tight transition state. Since $k_{orb}(E,J)$ is independent of this barrier the overall reaction rate constant, $k_{products}$ will depend strongly on $\Delta E^{\ddagger}$.

The probability of product formation is simply $k_{products}/k_{collision}$. Phase space theory calculations of this ratio are shown in Figure 7 for Co^+/C_3H_8 as a function of the relative barrier height $\Delta E^{\ddagger}$.

When $\Delta E^{\ddagger} \rightarrow 0$, $k_{products}/k_{collision} \rightarrow 0$ and essentially no reaction occurs. As the height of the tight transition state drops below the asymptotic energy of the reactants, $\Delta E^{\ddagger}$ increases and $k_{products}/k_{collision}$ starts to increase. As can be seen in Figure 7, reaction occurs on essentially every collision for $\Delta E^{\ddagger} \geq 1.0$ eV.

The ion beam data in Figure 2 indicate that reaction occurs on approximately 13 ± 5% of the collisions for Co^+/propane. This point is indicated by the arrow in Figure 7. For this value of $k_{products}/k_{collision}$, $\Delta E^{\ddagger} = 0.11 \pm 0.03$ eV. The error bars include both the uncertainty in the measurement and the uncertainty in the theory (related to choosing the precise structure and vibrational frequencies of the transition state).

2. Isotope Effects on Reaction Cross Sections. Both methane and hydrogen elimination channels are reduced by the same amount for Co^+ reacting with C_3D_8 relative to C_3H_8 at the lowest energies. This is strong evidence that the rate-limiting step is the same for both channels and that a C–H bond is almost certainly involved in this process. In the preceding section a model was developed that rationalized the 13 ± 5% efficiency of Co^+ reacting with C_3H_8 as due to a C–H insertion barrier located 0.11 ± 0.03 eV below the entrance channel asymptotic energy. That same model, if correct, should also quantitatively explain the observed isotope effect.

Several years ago we developed a model for explaining large isotope effects in reactions of NH_2^- and OH^- with ethyl ether.[26] Those systems are directly analogous to Co^+/propane in that a C–H (C–D) bond activation is proposed to be rate limiting. The maximum difference in the transition-state energies for the protonated and deuterated systems is simply the difference in zero point energies for the C–H and C–D bonds.

$$\Delta E^{\ddagger}_H - \Delta E^{\ddagger}_D = \tfrac{1}{2}h(\nu_{CH} - \nu_{CD}) = 0.047 \text{ eV} \quad (4)$$

When this energy shift is incorporated into the phase space calculations for $Co(C_3H_8)^+$ (along with appropriately changing all the frequencies and the rotational constant for deuteration), the theoretical prediction is

$$\gamma(C_3H_8)/\gamma(C_3D_8) = 2.6 \pm 0.4 \quad (5)$$

where $\gamma = k_{products}/k_{collision}$. This result is in excellent agreement with experiment (2.8 ± 0.8) and serves as a confirmation of the proposed model. The fact that the full C–H (C–D) isotope shift was required to obtain agreement between experiment and theory indicates it is the C–H rather than the C–C bond which is involved in the rate-limiting transition state.

A strong decrease in the total cross section is observed for all the isotopic variants, as the extent of deuteration increases. To analyze these trends in detail requires knowledge of the site specificity of the initial insertion process. The magnitude of the decrease relative to the C_3D_8 result is consistent with the number of C–H bonds which are deuterated. This point will be discussed in more detail in section IV.C.

B. Metastable Dissociation of Nascent $Co(C_3H_8)^+$ Complexes. 1. CH_4 Loss. The kinetic energy release distribution for methane elimination (Figure 5) is *narrower* than the statistical result. This is unusual since most nonstatistical processes yield kinetic energy release distributions *broader* than the statistical prediction. Distributions which are narrower than the statistical result will be referred to as translationally cold. In general, the kinetic energy release distribution is most sensitive to features of the potential surface near the exit channel.[12,19] Exit channel effects cannot be responsible for translationally cold products, however. If the exit channel has a reverse activation barrier, the products will be translationally hot. If there is no barrier, then the statistical result should be observed. Consequently, we suggest aspects of the potential energy surface remote from the exit channel are responsible.

In the previous sections, a theoretical model was developed that simultaneously explained both the magnitude of the observed cross section and the observed isotope effect. The evidence indicates

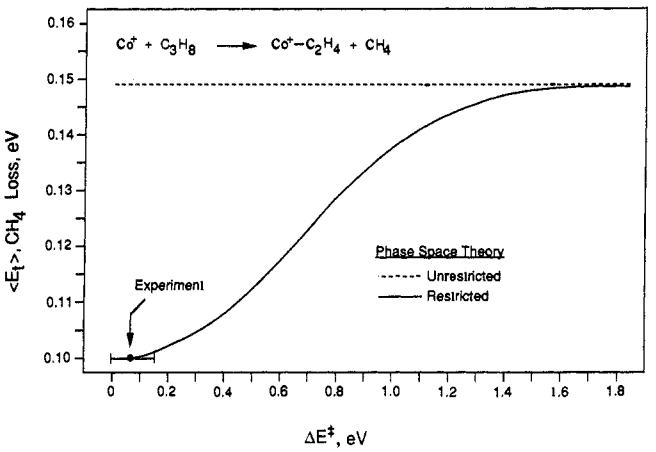

Figure 8. A plot of the average kinetic energy release, $\langle E_t \rangle$, versus $\Delta E^{\ddagger}$ (defined in Figure 6) for the reaction $Co^+ + C_3H_8 \rightarrow Co(C_2H_4)^+ + CH_4$. The "unrestricted" phase space theory result (dashed line) assumes the tight transition state for C–H insertion is not involved in the reaction. The "restricted" phase space theory result (solid line) incorporates the C–H insertion barrier into the analysis.

that the initial step in both CH_4 loss and H_2 loss was C–H bond insertion and that this step was rate limiting. If this conclusion is correct then the probability of passage through the C–H insertion transition state defines the energy and angular momentum distribution that will ultimately be responsible for product formation.

For CH_4 loss the general appearance of the product kinetic energy distribution is suggestive of a statistical release, peaking at low energy and falling off quasiexponentially to zero. As shown in Figure 5, however, a full phase space theory treatment using the E,J distributions created by passage through the orbiting transition state in the entrance channel is much broader than experiment. Using the model developed earlier in this paper (Section IV.A.1., Figure 6) we can recalculate the kinetic energy release distribution by implementing a barrier for C–H insertion involving a tight transition state (see Appendix for details). The average kinetic energy release, $\langle E_t \rangle$, calculated as a function of the barrier height, $\Delta E^{\ddagger}$, is shown in Figure 8 for Co^+/C_3H_8. The experimental value of $\langle E_t \rangle_{exp} = 0.099 \pm 0.003$ eV (Table IV) suggests $\Delta E^{\ddagger}$ is between 0 and 0.15 eV below the asymptotic energy of the reactants. This is consistent with the more exact barrier height, $\Delta E^{\ddagger} = 0.11 \pm 0.03$ eV, obtained by fitting the relative reaction cross section, $k_{products}/k_{collision}$ (Figure 7).

We noted previously that values of $\Delta E^{\ddagger} \geq 1.0$ eV result in reaction on essentially every collision (Figure 7). Comparison of Figure 7 with Figure 8 indicates, however, that the predicted kinetic energy release approaches the full phase space theory prediction more slowly than the predicted reaction efficiency.

A more sensitive comparison of experiment and theory is in the actual kinetic energy release distributions themselves. The distribution predicted by the theoretical model for CH_4 loss at $\Delta E^{\ddagger} = 0.11$ eV is given in Figure 5. Clearly the fit to the experimental data is excellent. This result is fully consistent with the analysis of the absolute cross section and isotope effects. The fact that the KERD for the CH_4-loss channel is shown to be statistical also provides very strong evidence that the final transition state is an orbiting transition state and that the $Co(C_2H_4)(CH_4)^+$ complex corresponds to a distinct minimum on the potential energy surface.[12b] A schematic reaction coordinate diagram depicting this effect and other known aspects of the potential energy surface is given in Figure 9.

If the microcanonical (E,J) values of the $k_{products}/k_{collision}$ calculation are examined, it becomes clear that the principal effect of the C–H insertion transition state is to bias against formation of products from collisions with high J values. This is a reasonable result since angular momentum increases the energy of the tight transition state more than it does that of the loose orbiting transition state (see Figure 9). Loss of the higher J portion of the (E,J) distribution results in products with less kinetic energy

(26) Bierbaum, V. M.; Filley, J.; DePuy, C. H.; Jarrold, M. F.; Bowers, M. T. *J. Am. Chem. Soc.* **1985**, *107*, 2818.

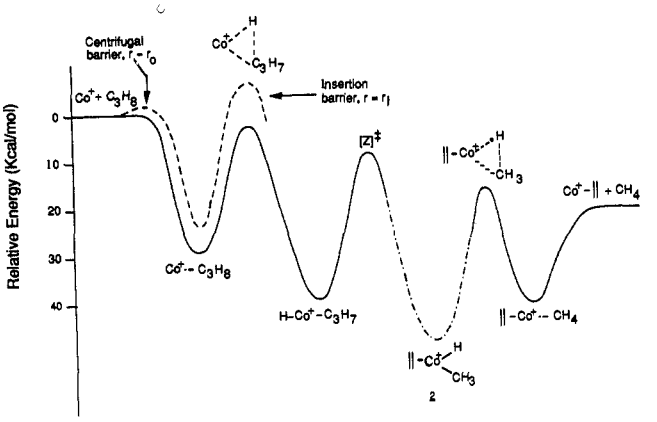

Figure 9. Schematic reaction coordinate diagram for the reaction $Co^+ + C_3H_8 \rightarrow Co(C_2H_4)^+ + CH_4$. The various structures the system assumes along the reaction path are shown. The dashed portion (– – –) schematically shows the effect of angular momentum on the initial orbiting transition state and the tight C–H insertion transition state. The dot-dash portion (· – ·) indicates uncertainty about whether the $C_2H_4Co^+(H)CH_3$ structure actually corresponds to a minimum along the potential energy surface. The transition state labeled $[Z]^‡$ is the point along this surface where insertion of Co^+ into the carbon skeleton of C_3H_8 occurs, ultimately leading to the demethanation products. Competition between this transition state and the one marked $[Y]^‡$ in Figure 11a leads to the branching between CH_4 loss and H_2 loss in the products. The transition state $[Z]^‡$ and the final transition state may be the same if $C_2H_4Co^+(H)CH_3$ is not stable to rearrangement.

than would have been expected if the full (*E,J*) distribution were available.

The metastable branching ratios given in Table III bring up a number of points deserving comment regarding the methane-loss channel. First, the fraction of $[Co(propane)^+]^‡$ complexes returning to reactants increases dramatically as the extent of deuteration increases. This result is consistent with the absolute cross-section data, and with our theoretical model of the isotope effect that indicates the tight transition state energy (leading to products) increases with deuteration but the orbiting transition state (leading back to reactants) does not. Second, the dehydrogenation channel decreases as the extent of deuteration increases for both the primary and secondary hydrogens, whereas the demethanation channel decreases only when the primary hydrogens are involved.

Another interesting point is that CH_3D loss is essentially not observed for Co^+ reacting with $CH_3CD_2CH_3$, indicating that methane loss is dominated by insertion into a primary C–H bond followed by β-CH_3 transfer as suggested in Scheme I. This result rules out equilibria between the hydrido–methyl–ethene intermediate **2** and the methyl–ethyl intermediate **3** in the CH_4-loss process. The present experiments provide no evidence for the

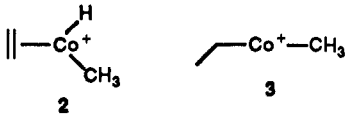

2 **3**

existence of the hydrido–methyl species **2** as a minimum on the potential energy surface. Methane elimination may in fact involve a multicenter transition state similar to that invoked below for H_2 elimination.

2. 1,2-Hydrogen Elimination. In contrast to the CH_4-loss channel, the observed kinetic energy release distribution for H_2 loss from Co^+/propane is clearly nonstatistical (Figure 4). For H_2 loss, the experimental kinetic energy release distribution is much broader than theory and has pronounced bimodality. The broad kinetic energy release indicates that a tight transition state near the exit channel for formation of the H_2-elimination products. A bimodal distribution almost always signifies two distinct decomposition processes. As shown in Scheme I, both primary and secondary C–H bond activation followed by β-H transfers are possible mechanisms for H_2 elimination, as suggested by previous

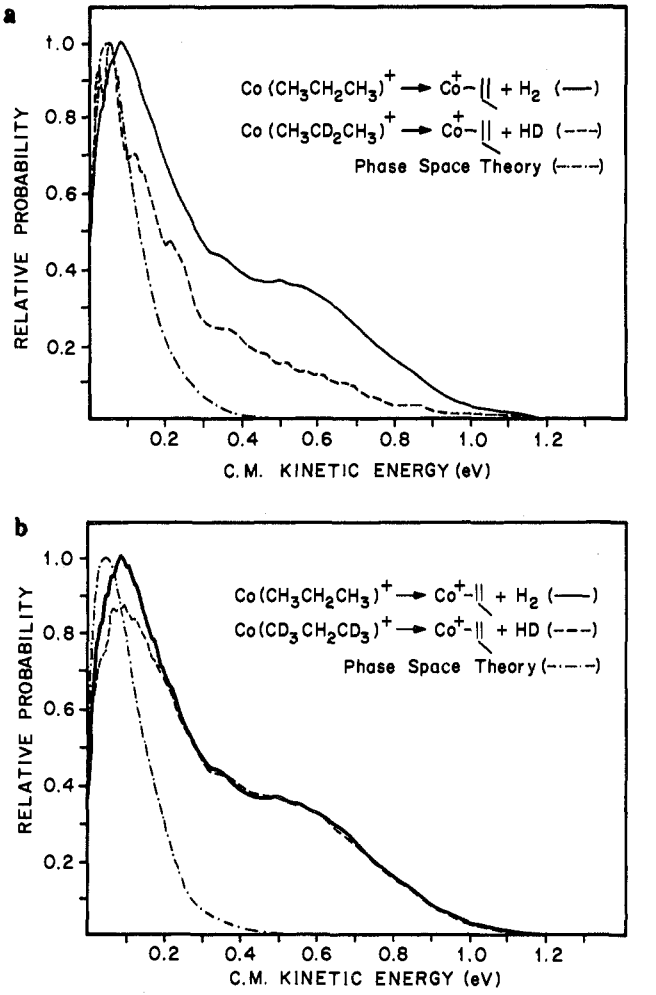

Figure 10. (a) Product kinetic energy release distributions for metastable loss of H_2 from nascent $Co(C_3H_8)^+$ (solid line) and HD from nascent $Co(CH_3CD_2CH_3)^+$ (dashed line). The phase space theory prediction is given by the dash-dot line. (b) Kinetic energy release distributions for metastable loss of H_2 from $Co(C_3H_8)^+$ (solid line) and HD loss from $Co(CD_3CH_2CD_3)^+$ (dashed line).

results.[2,5-7] The question is whether these two mechanisms are responsible for the bimodal kinetic energy release distribution in the Co^+/propane system.

In order to gain some insight into the details of the mechanism, kinetic energy release distributions using propane-*2,2-d*$_2$, propane-*1,1,1-d*$_3$, propane-*1,1,1,3,3,3-d*$_6$, and propane-*d*$_8$ were obtained. The kinetic energy release distributions for HD loss from Co^+ reacting with propane-*2,2-d*$_2$ and propane-*1,1,1,3,3,3-d*$_6$ are shown in Figure 10, parts a and b, along with H_2 loss from $Co(C_3H_8)^+$. For propane-*2,2-d*$_2$, the high-energy component in the kinetic energy release distribution is substantially reduced for HD loss in comparison to H_2 loss. For propane-*1,1,1,3,3,3-d*$_6$, however, the low-energy component is significantly reduced for HD loss in comparison to H_2 loss from C_3H_8. These results can be understood in the following way. Since both primary and secondary C–H bond activation are possible, either the metal ion initially inserts into a primary C–H(D) bond, followed by secondary C–H(D) bond activation, or a secondary C–H(D) bond is initially activated followed by a primary C–H(D) bond cleavage.

This sequence of events is shown graphically in Figure 11. The substantial reduction of the low- and high-energy components when D replaces H in the primary and secondary positions in propane (Figure 10) unambiguously indicates that the initial primary and secondary C–H(D) insertion barriers are both near the asymptotic energy of the reactants. The increase in energy of either transition state (by up to 0.047 eV) when D replaces H strongly reduces the flux through it relative to the C–H insertion transition state it competes with.

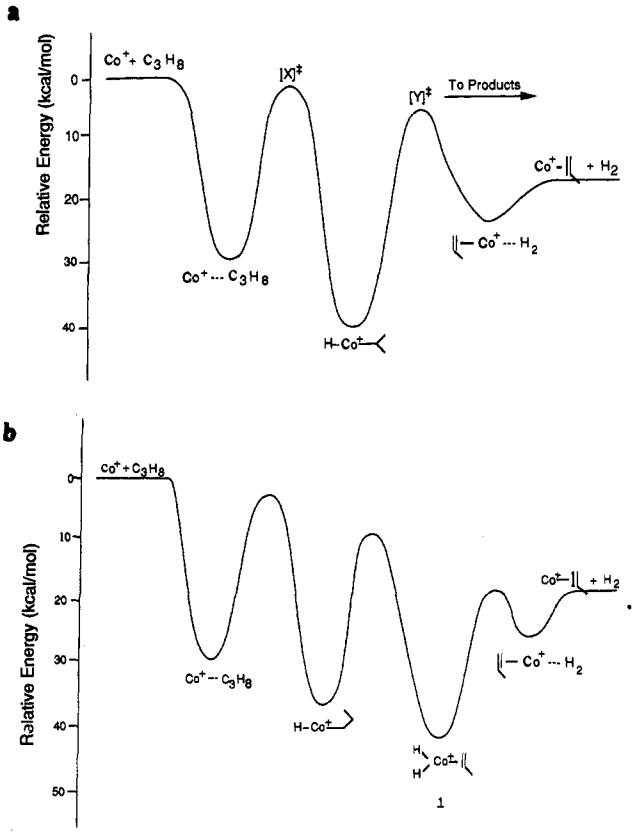

Figure 11. (a) Schematic reaction coordinate diagram for the reaction $Co^+ + C_3H_8 \rightarrow Co(C_3H_6)^+ + H_2$ involving initial secondary C–H bond activation. The transition state marked $[X]^‡$ is identical with the "insertion barrier" in Figure 9 and Figure 11, parts a and b, and is rate determining for all three reaction channels. The transition state marked $[Y]^‡$ competes with the transition state labeled $[Z]^‡$ in Figure 9 leading to the branching ratio between CH_4-loss and H_2-loss products. No distinction is made between initial primary or secondary C–H insertion for simplicity. (b) Schematic reaction coordinate diagram for the reaction $Co^+ + C_3H_8 \rightarrow Co(C_3H_6)^+ + H_2$ involving initial primary C–H bond activation.

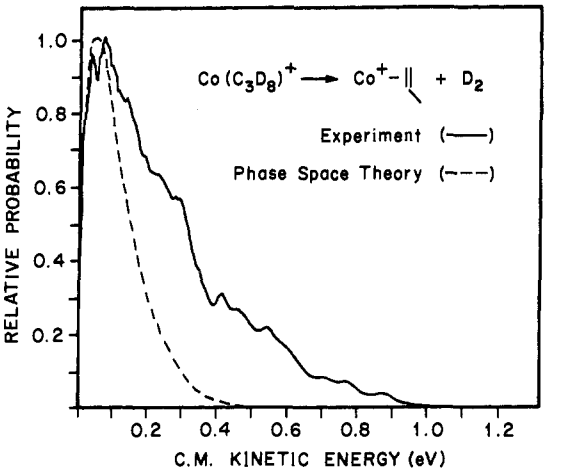

Figure 12. Product kinetic energy release distribution for metastable loss of D_2 from the nascent $Co(C_3D_8)^+$ collision complex (solid line). The phase space theory prediction is given by the dashed line.

Scheme II

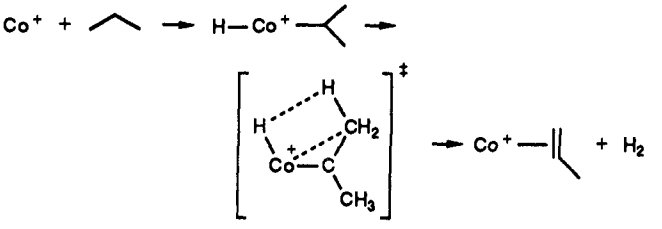

The difference in energy between high- and low-energy components in the KERD for dehydrogenation is quite large, approximately 0.4 eV. The high-energy component is much broader than the statistical distribution, suggesting a large barrier in the exit channel. The low-energy component, however, appears to be nearly statistical. For HD loss from $Co(CH_3CD_2CH_3)^+$, the substantial reduction in the high-energy component effectively deconvolutes the two decomposition processes in the KERD such that the low-energy component now appears statistical (see Figure 10a). The theoretical kinetic energy release distribution for H_2 elimination (Figure 10a) was calculated with and without implementation of a barrier for C–H insertion. The significant angular momentum restriction observed for methane elimination (Figure 5), due to the C–H insertion barrier, is not observed for H_2 elimination (i.e. the statistical kinetic energy release distribution is not translationally cold for H_2 loss). This is because loss of H_2 from the $Co(C_3H_8)^+$ complex is already restricted to low angular momenta, due to the low mass and polarizability of H_2, independent of restrictions imposed by the C–H insertion transition state. As a result, the effect of angular momentum on the initial orbiting transition state and tight C–H insertion transition state shown in Figure 9 is much less for H_2 elimination than for CH_4 elimination.

The mechanism for dehydrogenation proposed in Scheme I is not consistent with these data. If both decomposition pathways go through the same dihydride intermediate, **1**, then the kinetic energy release distribution would be independent of the initial site of insertion. An alternative mechanism which is consistent with all the data including the observed isotope effects is as follows. *Initial* secondary C–H bond activation may be followed by a multicenter H_2 elimination[27] as shown in Scheme II and Figure 11a. One would expect a large kinetic energy release for this process giving rise to the high-energy component of the KERD. *Initial* primary C–H bond activation, on the other hand, may be followed by β-H transfer forming the dihydride intermediate, **1** (Scheme I), prior to H_2 elimination as shown in Figure 11b. This process would then correspond to the small, nearly statistical kinetic energy release.

The kinetic energy release distribution for D_2 loss from $Co(C_3D_8)^+$ is shown in Figure 12. The signal intensity was much weaker, making the analysis of these results more difficult. The overall much weaker signal is consistent with an increased insertion barrier for C–D bond activation relative to C–H bond activation at both primary and secondary sites.

For larger systems the initial electrostatic well is deeper and consequently the C–H insertion barrier is reduced in energy. A consequence of lowering the C–H insertion barrier relative to the energy of the reactants is that isotope effects *on the reaction cross section or rate* will cease being significant. Their interpretation will not be complicated by subtle potential surface effects, instead they will simply indicate which hydrogen atoms are involved in an H_2 elimination reaction. Such is the case, for example, for reactions of Co^+ with *n*-butane and *n*-butane-*1,1,1,4,4,4-d*$_6$.[12] In these systems the H_2 elimination reaction is fast with a rate essentially independent of deuterium labeling, indicating the C–H insertion barrier is substantially below the asymptotic energy of the reactants.

An interesting comparison of these results is with the results of Schulze and Schwarz.[28] These authors reported KERDs for Mn^+-induced dehydrogenation of deuterated 4-octyne, 1,2-HD elimination from $CD_3(CH_2)_2C{\equiv}CC_3H_7$, and 2,3-HD elimination from $CH_3CH_2CD_2C{\equiv}CC_3H_7$. In the first process, Schulze and Schwarz see a bimodal KERD, while in the second, the KERD

(27) Theoretical support for multicenter H_2 elimination is found in: (a) Steigerwald, M. L.; Goddard, W. A. *J. Am. Chem. Soc.* **1984**, *106*, 308. (b) Low, J. J.; Goddard, W. A. *J. Am. Chem. Soc.* **1984**, *106*, 6928. Low, J. J.; Goddard, W. A. *J. Am. Chem. Soc.* **1984**, *106*, 8321.

(28) Schulze, C.; Schwarz, H. *Int. J. Mass Spectrom. Ion Proc.* **1989**, *88*, 291.

has only a single, narrow component. We suggest that the bimodal KERD can be explained in direct analogy with the Co^+-induced elimination of H_2 from propane as discussed above. The 1,2-HD elimination occurs by two pathways: initial insertion into a secondary C–H bond followed by final breaking of a primary C–D bond before going to products, or initial insertion into the primary C–D bond followed by secondary C–H bond breaking. Then the high-energy component in the KERD for 1,2-HD elimination reported by Schultze and Schwarz corresponds to *final* breaking of a primary C–H(D) bond since this is what we observe in the propane case. For Mn^+-induced 2,3-HD loss from $CH_3CH_2C{-}D_2C{\equiv}CC_3H_7$, the KERD arises exclusively from initial secondary C–H(D) insertion followed by secondary C–H(D) bond breaking as the HD elimination products evolve. Hence, it seems to be a common feature that the transition state associated with a *final* secondary C–H bond breaking is lower in energy than the corresponding *final* primary C–H bond breaking transition state. Other dynamical factors could, of course, be involved and the generality of this result awaits further experimentation.

C. Branching Ratios for Co^+/Propane. Evidence has been presented that at low kinetic energy CH_4 loss proceeds through a rate-determining transition state involving initial primary C–H bond activation. H_2 loss, however, proceeds via both initial primary and initial secondary C–H bond activation, with each exhibiting a rate-limiting transition state. The branching ratios for all the isotopic variants shown in Figure 3 and Table II support these results. Deuterating the secondary carbon decreases the fraction of dehydrogenation relative to demethanation since the fraction of initial secondary C–H insertion will decrease upon deuteration, and this affects only the dehydrogenation channel. Deuterating the end carbons, however, increases the fraction of dehydrogenation at the expense of demethanation since demethanation requires primary C–H bond activation which is suppressed upon deuteration.

For $CH_3CH_2CD_3$, the ~2:1 branching ratio for CD_3H to CH_3D loss is consistent with initial primary C–H bond activation being attenuated upon deuteration since CD_3H elimination involves initial C–H bond activation, whereas CH_3D elimination involves initial C–D bond activation.

D. Location of the Rate-Limiting Transition State. To this point the data presented in this paper are consistent with initial C–H bond activation as the rate-limiting transition state for both CH_4 and H_2 elimination channels. Recent measurements of binding energies and clustering kinetics of Co^+ with methane and ethane,[29] as well as threshold collisional activation studies[30] of the corresponding adducts, further support this conclusion. For example, CID of the $Co(CH_4)^+$ and $Co(C_2H_6)^+$ adducts yield Co^+ almost exclusively at all energies. Consequently, insertion of Co^+ into a C–H bond in these molecules does not occur at thermal energy. In other words, it is the initial C–H bond activation energy barrier which prevents H_2 elimination from occurring in the Co^+/C_2H_6 system, even though this process is known to be exothermic by 11 kcal/mol. The increased polarizability of propane lowers the C–H bond activation energy barrier enough to observe both hydrogen and methane elimination products at thermal energies. Measuring the binding energies of Co^+ with propane and deuterated propanes will give additional insight into the nature of this rate-limiting transition state.

The bimodal nature of the KERD for H_2 elimination indicates two distinct decomposition processes are present. Since deuteration of the end carbons, $CD_3CH_2CD_3$, decreases the low-energy component, it must be initial primary C–H bond activation which is rate limiting for the low-energy component in the KERD. Deuterating the center carbon, $CH_3CD_2CH_3$, decreases the high-energy component in the KERD. The rate-limiting transition state in this case must be initial secondary C–D insertion since this is the only step in the reaction which involves a deuterium rather than a hydrogen. Thus, both initial primary and secondary C–H bond activation are rate-limiting transition states for the dehydrogenation channel.

Table V. Input Parameters Used in Calculations

	H_2	HD	D_2	CH_4	CD_4	C_3H_8	C_3D_8
$\Delta H_{f_0}{}^{\circ a}$	0	0	0	−15.97	−15.97	−19.4	−19.4
B^b	60.86	45.65	30.43	5.24	2.64	0.409	0.300
σ^c	2	1	2	12	12	2	2
α^d	0.808	0.812	0.796	2.56	2.56	6.14	6.14
$\nu_i{}^e$	4395	3817	3118	2917	2109	2977	2225
				1534 (2)	1092 (2)	2962	2122
				3019 (3)	2259 (3)	2887 (2)	2081 (2)
				1306 (3)	996 (3)	1476	1086 (2)
						1462	1064 (4)
						1392	959
						1158	712
						869	332
						369	2221
						2967	945
						1451	659
						1278	143
						940	2224 (2)
						216	1203
						2968 (2)	1068
						1464	862
						1378	688
						1338	2149
						1054	949
						922	544
						2973	172
						1472	
						1192	
						748	
						268	

[a] Heat of formation at 0 K in kcal/mol. [b] Rotational constant in cm^{-1}. [c] Symmetry number. [d] Polarizability in Å^3. [e] Vibrational frequencies in cm^{-1}.

The mechanism for demethanation involves either initial primary C–H bond activation followed by β-CH_3 transfer or initial C–C bond activation followed by β-H transfer. From the analysis of the dehydrogenation channel, we know that initial primary C–H bond activation does occur. In addition, at low kinetic energy, the decrease in cross section for C_3D_8 relative to C_3H_8 is exactly the same for demethanation as it is for dehydrogenation, suggesting initial C–C bond insertion is not likely to prevail at low energy. Finally, demethanation becomes the dominant channel at higher kinetic energies consistent with initial C–H bond activation being prevalent at low kinetic energy and initial C–C bond activation becoming available at higher kinetic energies. The final transition state for demethanation, shown in Figure 9, is not likely to be rate limiting, as suggested in ref 2d, since this would give rise to a large nonstatistical kinetic energy release, whereas a very narrow statistical KERD is observed. Thus, at thermal energy, initial primary C–H bond activation must be the rate-limiting transition state for the demethanation channel.

E. Excited Electronic States. The evidence presented up to this point strongly supports the existence of two distinct mechanisms for H_2 elimination on the ground-state surface. However, the possibility that excited electronic states of cobalt reactant ions contribute to the bimodal character of the kinetic energy release distribution must also be considered. $Co(CO)_3NO$ is known to give only 34% ground-state Co^+ under electron impact conditions (≥40 eV).[31] $CoCp(CO)_2$, however, gives ~90% ground-state Co^+ with electron impact (≤40 eV).[31] To examine the effect of excited electronic states in Co^+ on the formation of the $Co(C_3H_8)^+$ complex and its subsequent dissociation, a comparison of results using both $Co(CO)_3NO$ and $CoCp(CO)_2$ was made. In the present study, no change in the shape of the KERD was observed, indicating the bimodal character of the H_2 loss KERD is almost certainly not due to reactions of different electronic states. Additionally, if the formation and reaction of electronically excited cobalt ions was the primary contributor to the bimodal KERD, then one would expect very similar distributions for metastable

(29) van Koppen, P. A. M.; Kemper, P. R.; von Helden, G.; Bowers, M. T. To be published.
(30) Haynes, C.; Fisher, E. R.; Armentrout, P. B. Work in progress.
(31) Kemper, P. R.; Bowers, M. T. *J. Am. Chem. Soc.* **1990**, *112*, 3231.

Table VI. Input Parameters Used in Calculations

	$CH_3CD_2CH_3$	d_1-Co$^+$ —‖	d_8-Co$^+$ —‖	d_4-Co$^+$ —‖	Co$^+$--C_3H_8[a]	Co$^+$--C_3D_8[a]
$\Delta H_{f_0}°$	−19.4	247	247	255	261[b]	262[b]
B	0.409	0.153	0.140	0.256	0.26[c] (0.093)[d]	0.20[c] (0.079)[d]
σ	2	1	1	2	1	1
α	6.14					
ν_i	2974 (2)	3090	3090	2251	2962[e]	2122[e]
	2883 (2)	3013	3013	1515	2887 (2)	2081 (2)
	2141	2991	2991	981	1476	1086 (2)
	1459	2954	2954	728	1462	1064 (4)
	1392	2932	2932	2304	1392	959
	1207	2871	2871	1009	1158	712
	1064	1650	1650	720	869	332
	843	1470	1470	780	369	2221
	362	1443	1443	2345	2967	945
	2956	1420	1420	586	1451	659
	1453	1378	1378	2200	1278	143
	1083	1297	1297	1078	940	2224 (2)
	777	1171	1171	500	216	1203
	208	1045	1045	600	2968 (2)	1068
	1461	991	991	700	1464	862
	1374	963	963		1378	688
	1203	920	920		1338	2149
	964	912	912		1054	949
	829	578	578		922	544
	2963	428	428		2973	172
	2182	174	174		1472	700
	1476	700	700		1192	600
	1146	600	600		748	500
	622	500	500		268	
	217				800	
					700	
					600	

[a] C–H(D) bond activation transition state complex. [b] Rough estimate. Calculated assuming $\Delta E^*(C_3H_8) = 0.11$ eV and $\Delta E^*(C_3D_8) = 0.06$ eV. [c] Rotational constant assuming Co$^+$ inserts into the C–H bond in the plane of propane. [d] Rotational constant assuming Co$^+$ inserts into the C–H bond perpendicular to the plane of propane. [e] One C–H(D) frequency becomes the reaction coordinate, breaking the C–H(D) bond. Hence, the number of frequencies, $\nu_i = 3N - 7$ where N is the number of atoms in the molecule.

dissociations of Co$^+$/complexes for propane and all the isotopically labeled variants. Specifically, if only *one* mechanism for H_2 loss was operative and if one assumed that the high-energy channel was solely due to the reactions of electronically excited cobalt ions, then one would not expect the strong isotope effects observed in Figure 10a. The high-energy channel is considerably reduced in the distribution for the complexes containing deuterium-labeled propane, indicating that the reaction pathway is sensitive to the zero point energy changes resulting from simple substitution of D for H. This is not the type of behavior consistent with an excited electronic state effect. Thus, at least two mechanisms must contribute to the formation of the dehydrogenation product ions exclusive of effects of electronically excited cobalt ions.

V. Conclusions

Kinetic energy release distributions, metastable product distributions, and absolute reaction cross-section measurements for both isotopically labeled and unlabeled propanes are used to provide mechanistic and dynamical information for transition-metal-mediated gas-phase reactions. The results are consistent with the schematic potential energy diagrams for CH_4 loss and H_2 loss from Co$^+$/(propane) as shown in Figures 9 and 11.

The observed isotope effects for deuterated propanes indicate that initial insertion into a C–H bond is rate limiting and no evidence exists for initial C–C bond insertion at low kinetic energies. For dehydrogenation, initial primary and secondary C–H bond activation give rise to low- and high-energy components in the bimodal kinetic energy release distribution, respectively. The high-energy component observed is broad relative to the predicted statistical kinetic energy release, consistent with a barrier in the exit channel. The origin of the barrier responsible for this component in the KERD is assigned to a concerted H_2-elimination mechanism. The low-energy component appears to be very nearly statistical, indicating a relatively smooth transition to products in the exit channel.

For demethanation, the barrier associated with the initial insertion of the metal ion into a C–H bond of propane restricts the total angular momentum available to the products yielding a translationally cold kinetic energy release distribution. The presence of this barrier is consistent with measured reaction cross sections which are substantially smaller than calculated Langevin collision cross sections. The cross-section data suggest initial primary C–H bond insertion is involved in CH_4 loss at low kinetic energies and that initial C–C bond insertion becomes available as the energy is increased.

Theoretical modeling allows determination of the energy of the rate-limiting C–H bond insertion transition state. The transition state was found to be located 0.11 ± 0.03 eV below the Co$^+$/C_3H_8 asymptotic energy. The transition states for primary and secondary C–H insertions appear to be very close in energy. The deduced tight transition state at $\Delta E^* = 0.11$ eV for C–H insertion is consistent with isotopic substitution results. If the full effect of C–H versus C–D bond breaking is employed in determining the zero-point energy of the transition states, the observed decrease in cross section on deuteration (a factor of 2.8) is matched by theory.

Finally, we have shown for the first time that kinetic energy release distributions can be very sensitive probes of features of the potential energy surface near the entrance channel, in addition to their well-known sensitivity to features of the exit channel.

These results are not unique to the Co$^+$/propane system. Similar results have been observed for Fe$^+$ reacting with propane. However, subtle and important differences exist in the Fe$^+$/propane system subject to further investigation.[32]

(32) van Koppen, P. A. M.; Bowers, M. T.; Beauchamp, J. L.; Armentrout, P. B. To be published.

(33) (a) Shimanouchi, T. *Table of Molecular Vibrational Frequencies Consolidated*; National Bureau of Standards: Washington, DC, 1972; Vol. I. (b) Sverdlov, L. M.; Kovner, M. A.; Krainov, E. P. *Vibrational Spectra of Polyatomic Molecules*; Wiley: New York, 1970.

Acknowledgment. The authors gratefully acknowledge the support of the National Science Foundation under Grants CHE88-17201 (MTB), CHE87-11567 (JLB), and CHE89-17980 (PBA). J.L.B. also thanks the donors of the Petroleum Research Fund, administered by the American Chemical Society. One of us (J.B.-L.) also thanks the National Science Foundation for a postdoctoral fellowship. We also acknowledge important discussions with Drs. Martin Jarrold and Marina Rincon regarding the theoretical calculations.

Appendix A

The model for statistical phase space calculations, applied to organometallic systems, has been previously outlined.[12b] In these calculations the kinetic energy distribution of product ions was obtained for comparison with experiment. In all instances the collision complex was formed through an orbiting transition state and dissociated to products via an orbiting transition state. Here we extend the calculations to include the effect of coupled transition states along the reaction coordinate on the kinetic energy release distributions and on reaction cross sections. The model is applied to reactions of Co^+ with propane and propane-d_8. The potential energy surface used in the calculations is shown in Figure 6. Competition occurs for the $Co(C_3H_8)^+$ complex between dissociation back to reactants (via the orbiting transition state) and to products via a tight transition state.

The probability of an Co(propane)$^+$ complex with energy E and angular momentum J forming products in channel i is given by expression (A1), where $F^{orb}(E,J)$ is the microcanonical flux

$$P_i(E,J) = \frac{F_i^{\ddagger}(E,J)}{F^{orb}(E,J) + F_i^{\ddagger}(E,J)} \quad \text{(A1)}$$

through the orbiting transition state back to reactants and $F_i^{\ddagger}(E,J)$ is the flux through the tight transition state to go on to products in channel i. Averaging over the E,J distribution resulting from a Co^+ + propane collision, the probability for forming products in channel i with translational energy E_t is given by (A2), where

$$P(E_t) = \left[\int_0^{\infty} dE\, e^{-E/kT} \int_0^{J_{max}} dJ 2J \times F_{in}^{orb}(E,J) \frac{F_i^{\ddagger}(E,J)}{F^{orb}(E,J) + F_i^{\ddagger}(E,J)} P_i(E,J;E_t) \right] \Big/ \left[\int_0^{\infty} dE\, e^{-E/kT} \int_0^{J_{max}} dJ 2J\, F_{in}^{orb}(E,J) \right] \quad \text{(A2)}$$

$F_{in}^{orb}(E,J)$ is the flux through the orbiting transition state to form the collision complex $Co(C_3H_8)^+$ and $P_i(E,J;E_t)$ is the fraction of molecules at energy E and angular momentum J decaying through the orbiting transition state to yield products i with translational energy E_t.

The bimolecular rate constant for formation of product i, $k_i(E,J)$, is given by eq A3, where $\rho(E,J)$ is the microcanonical

$$k_i(E,J) = F_{in}^{orb}(E,J) \left[\frac{F_i^{\ddagger}(E,J)}{F^{orb}(E,J) + F_i^{\ddagger}(E,J)} \right] \Big/ \rho(E,J) \quad \text{(A3)}$$

density of states of the reactants. Averaging over the E,J distribution, the bimolecular rate constant relative to the total collision rate constant is

$$\frac{k_i}{k_{collision}} = \left[\int_0^{\infty} dE\, e^{-E/kT} \int_0^{J_{max}} dJ 2J \times F_{in}^{orb}(E,J) \frac{F^{\ddagger}(E,J)}{F^{orb}(E,J) + F^{\ddagger}(E,J)} \right] \Big/ \left[\int_0^{\infty} dE\, e^{-E/kT} \int_0^{J_{max}} dJ 2J\, F_{in}^{orb}(E,J) \right] \quad \text{(A4)}$$

$$\frac{k_{tot}}{k_{collision}} = \frac{\Sigma_i k_i}{k_{collision}} \quad \text{(A5)}$$

where k_{tot} is the total bimolecular rate constant for all product channels. Equation A2 is used for comparison with experimental kinetic energy release distributions and eq A4 and A5 for comparison with reaction cross-section measurements.

In order to calculate the kinetic energy distributions, structures and vibrational frequencies for the various species are required. These were taken from the literature where possible, or estimated from literature values of similar species.[33] The details of the kinetic energy distributions were found to vary only weakly with structure or vibrational frequencies over the entire physically reasonable range for these quantities. The distributions were strongly dependent on the total energy available to the dissociating complex, and hence in our model to the ΔH° of reaction. Often all heats of formation of products and reactants were well-known except one, the organometallic product ion. However, in this case, the heats of formation for $Co(C_3H_8)^+$ and $Co(C_2H_4)^+$ have been fairly well established.[12b] These heats of formation were consistently used throughout the calculations and are summarized along with the parameters in Tables V and VI.

Registry No. C_3H_8, 74-98-6; CH_3CHDCH_3, 20717-74-2; $CH_3CD_2CH_3$, 2875-95-8; $CD_3CH_2CH_3$, 2875-97-0; $CD_3CH_2CD_3$, 2875-96-9; C_3D_8, 2875-94-7; Co^+, 16610-75-6.